Optical properties of fat emulsions

René Michels, Florian Foschum, and Alwin Kienle

Institut für Lasertechnologien in der Medizin und Meßtechnik, Helmholtzstr. 12, D-89081 Ulm, Germany

rene.michels@ilm.uni-ulm.de

Abstract: We present measurements of the optical properties of six different fat emulsions from three different brands, Clinoleic, Lipovenoes and Intralipid, with fat concentrations from 10 % to 30 %. The scattering coefficient, the reduced scattering coefficent, and the phase function of each sample are measured for wavelengths between 350 nm and 900 nm. A method for the calculation of the particle size distribution of these fat emulsions is introduced. With the particle size distribution the optical properties of the fat emulsions are obtained with Mie theory. Simple equations for the calculation of the absorption coefficient, the scattering coefficient, the reduced scattering coefficient, the g factor, and the phase function of all measured samples are presented.

© 2008 Optical Society of America

OCIS codes: (290.3030 index measurements; 290.7050 turbid media)

References

1. A. Kienle, F. Forster, and R. Hibst, "Influence of the phase function on determination of the optical properties of biological tissue by spatially resolved reflectance," Opt. Lett. **26**, 1571–1573 (2001).
2. F. Martelli and G. Zaccanti, "Calibration of scattering and absorption properties of a liquid diffusive medium at NIR wavelengths. CW method," Opt. Express **15**, 486–500 (2007).
3. J. Allardice, A. M. Abulafi, D. Webb, and N. Willimas, "Standardization of intralipid for light scattering in clinical photodynamic therapy," Lasers Med. Sci. **7**, 461–465 (1992).
4. S. Flock, S. Jacques, B. Wilson, W. Star, and M. vanGemert, "The optical properties of Intralipid: a phantom medium for light propagation studies," Lasers Surg. Med. **12**, 510–9 (1992).
5. H. van Staveren, C. Moes, J. van Marle, S. Prahl, and M. Gemert, "Light scattering in Intralipid-10 in the wavelength range of 400-1100 nm," Appl. Opt. **30**, 4507–4514 (1991).
6. J. Choukeife and J. L'Huillier, "Measurements of scattering effects within tissue-like media at two wavelengths of 632.8 nm and 680 nm," Lasers Med. Sci. **14**, 286–296 (1999).
7. E. Drakaki, S. Psycharakis, M. Makropoulou, and A. Serafetinides, "Optical properties and chromophore concentration measurements in tissue-like phantoms," Opt. Commun. **254**, 40–51 (2005).
8. I. Driver, J. Feather, P. King, and J. Dawson, "The optical properties of aqueous suspensions of Intralipid, a fat emulsion," Phys. Med. Biol. **34**, 1927–1930 (1989).
9. S. Flock and B. W. M. Patterson, "Total attenuation coefficients and scattering phase functions of tissues and phantom materials at 633 nm," Med. Phys. **14**, 835–841 (1987).
10. A. Giusto, R. Saija, M. A. Iati, P. Denti, F. Borghese, and O. Sindoni, "Optical properties of high-density dispersions of particles: application to intralipid solutions," Appl. Opt. **42**, 4375–4380 (2003).
11. T. Pham, F. Bevilacqua, T. Spott, J. Dam, and B. T. S. Andersson-Engels, "Quantifying the absorption and reduced scattering coefficients of tissuelike turbid media over a broad spectral range with noncontact fourier-transform hyperspectral imaging," Appl. Opt. **39**, 6487–6497 (2000).
12. G. Zaccanti, S. Bianco, and F. Martelli, "Measurements of optical properties of high-density media," Appl. Opt. **42**, 4023–4030 (2003).
13. A. Kienle and M. Patterson, "Improved solutions of the steady-state and the time-resolved diffusion equations for reflectance from a semi-infinite turbid medium." J. Opt. Soc. Am. **14**, 246–254 (1997).
14. A. Kienle, L. Lilge, M. Patterson, R. Hibst, R. Steiner, and B. Wilson, "Spatially-resolved absolute diffuse reflectance measurements for non-invasive determination of the optical scattering and absorption coefficients of biological tissue," Appl. Opt. **35**, 2304–2314 (1996).

#92339 - $15.00 USD Received 1 Feb 2008; revised 18 Mar 2008; accepted 4 Apr 2008; published 11 Apr 2008

15. M. Pilz and A. Kienle, "Determination of the optical properties of turbid media by measurement of the spatially resolved reflectance," in *Proc. SPIE Int. Soc. Opt. Eng.* (2007).
16. F. Forster, A. Kienle, R. Michels, and R. Hibst, "Phase function measurements on nonspherical scatterers using a two-axis goniometer," J. Biomed. Opt. **11**, 024,018 (2006).
17. R. Michels, S. Boll, and A. Kienle, "Measurement of the phase function of phantom medias with a two axis goniometer," in *Photon Migration and Diffuse-Light Imaging* (SPIE, 2007).
18. D. Lide, *Handbook of chemistry and physics* (CRC, 2008).
19. C. Wabel, "Influence of lecithin on structure and stability of parental fat emulsions," Ph.D. thesis, University Erlangen, Germany (1998).
20. The International Association for the Properties of Water and Steam, "Release on the refractive index of ordinary water substance as a function of wavelength, temperature and pressure," (1997).
21. G. Mie, "Beitrage zur Optik trüber Medien, speziell kolloidaler Metallösungen," Ann. Physik **330**, 377–445 (1908).
22. R. Graaff, J. Aarnoudse, J. Zijp, P. Sloot, F. de Mul, J.Greve, and M. Koelink, "Reduced light-scattering properties for mixtures of spherical particles: a simple approximation derived from Mie calculations," Appl. Opt. **31**, 1370–1376 (1992).
23. R. Pope and E. Fry, "Absorption spectrum (380-700 nm) of pure water. II Integrating cavity measurements," Appl. Opt. **36**, 8710–8723 (1997).

1. Introduction

In recent years great effort has been made to improve the understanding of light propagation in turbid media. Better accuracy in diffuse optical tomography and spectroscopy can be achieved with enhanced measurement devices but likewise it will be achieved by improvements in the modeling of the light propagation in turbid media. Besides the modeling of the macroscopic structure of biological tissue also the consideration of the microscopic light interaction provides further advancement. For example, the use of the real phase function leads to a more precise prediction of the light propagation even in semi-infinite media [1]. In contrast to this demand, there is a lack of exact experimental data for the phase function and optical properties of the examined turbid media. Even for well examined calibration media like fat emulsions there are still exact measurements of the phase function missing.

Fat emulsions like Intralipid are frequently used in the research of light propagation in turbid media. These fat emulsions are similar to milk, consist of fat droplets suspended in water and are originally designated for parenteral nutrition of patients. In the field of diffuse imaging and spectroscopy, they are frequently used as calibration standards [2] for systems in clinical use [3] or as tissue models for the development of new methods. These fat emulsions offer some striking advantages over other calibration standards. They offer low absorption, have an easy adjustable scattering coefficient, are cheap and highly accessible in the clinical environment, they are sterile, homogeneous, non-toxic and they are available in big quantities. Due to their relevance they have been topic of many studies [4, 5, 6, 7, 8, 9, 10, 11, 12]. Besides the optical properties, the scattering coefficient μ_s, the reduced scattering coefficient μ_s', the absorption coefficient μ_a and the anisotropy factor g, also the particle size distribution of Intralipid [5, 6] has been reported in literature. In addition, there have been comparative studies of different fat emulsions with different fat concentrations [6].

Despite of all these studies, the direct measurements of the phase function was only topic of a few publications [6, 9]. The g factor was measured mostly indirectly by calculating it from the measurement of μ_s and μ_s'. In addition, the recipe and the manufacturing of Intralipid 10 % have changed since the study of van Staveren et al. [5] which is the most cited work concerning the optical properties of Intralipid 10 %. Consequently, the optical properties of Intralipid 10 % have changed. Furthermore, there are various different fat emulsions on the market today and each brand is also available in different fat concentrations. It shall be noted beforehand that great differences of the optical properties of fat emulsions of different brands and even of fat emulsions of the same brand with different fat concentrations were found.

#92339 - $15.00 USD Received 1 Feb 2008; revised 18 Mar 2008; accepted 4 Apr 2008; published 11 Apr 2008
(C) 2008 OSA

In this paper we present measurement of the optical properties, μ_s, μ_s', g, and the phase function $p(\theta)$, of Intralipid, Lipovenoes and ClinOleic, with fat concentrations from 10% to 30% for wavelengths between 350 nm and 900 nm. The size distribution of each fat emulsion was calculated and is presented here. With the given size distribution the optical properties can be computed with Mie theory. Due to the complexity of the Mie theory simple analytic equations are presented to calculate the optical properties, μ_a, μ_s, μ_s', g, as well as the phase function $p(\theta)$, for wavelengths from 400 nm to 1000 nm for each sample.

The paper is structured as follows. All experimental methods and all information needed for the calculation of the scattering properties of the fat emulsions with Mie theory are given in the methods and materials section. The measurement of μ_s and μ_a is explained in section 2.1, the measurement of μ_s' is stated in section 2.2 and the measurement of the phase function and the anisotropy factor is introduced in section 2.3. A brief introduction to the correction of the phase function measurement is given in section 2.4. The consistence and physical properties of the fat emulsions are explained in section 2.5. Mie theory is briefly introduced in section 2.6. The calculation of the size distribution is explained in section 2.7. In the result section we finally present the comparison of our measurement results with Mie theory. In section 3.1 two examples of the phase function measurements are discussed. The measurements of the anisotropy factor (section 3.2), of the scattering coefficient (section 3.3), of the reduced scattering coefficient (section 3.4) and of the absorption coefficient (section 3.5) follow. In section 3.6 analytical formulations for the calculation of μ_a, μ_s, μ_s', g and $p(\theta)$ are given.

2. Methods and materials

2.1. Collimated transmission setup

With the collimated transmission setup the scattering coefficient of fat emulsions and the absorption coefficient of soy bean oil can be measured within a broad wavelength range. This makes it a prominent technique to monitor the optical properties of calibration media for changes over time. With the collimated transmission setup the attenuation coefficient, $\mu_t(\lambda) = \mu_a(\lambda) + \mu_s(\lambda)$, of a sample is measured. In our setup the sample is illuminated with a collimated white light source. The measured intensity $I(\lambda)$ is described by the Lambert-Beer law:

$$I(\lambda) = I_0 \cdot e^{(-\mu_t(\lambda)\cdot c\cdot d)}, \tag{1}$$

where c is the concentration, d is the path length trough the sample, and I_o is the incident intensity. The distance between sample and detector has to be large enough to detect only unscattered photons. Then, the measured attenuation coefficient of solely scattering samples, $\mu_s \gg \mu_a$, equals the scattering coefficient, $\mu_t = \mu_s$, like it is the case for fat emulsions. For solely absorbing samples, $\mu_a \gg \mu_s$, the measured attenuation coefficient equals the absorption coefficient, $\mu_t = \mu_a$.

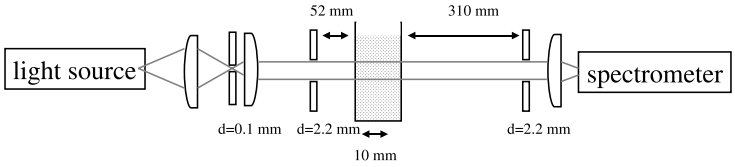

Fig. 1. Sketch of collimated transmission setup to measure the attenuation coefficient $\mu_t = \mu_a + \mu_s$.

In Fig. 1 a sketch of the setup is shown. Thermal light sources (e.g. Ocean Optics, wolfram

#92339 - $15.00 USD Received 1 Feb 2008; revised 18 Mar 2008; accepted 4 Apr 2008; published 11 Apr 2008
(C) 2008 OSA

halogen light source HL-2000) as well as laser sources (e.g. He-Ne laser and diode lasers) were employed. The collimation optics (lenses 1 and 2 and the first pinhole) are not necessary for laser sources. Two different spectrometers, an Ocean Optics PC 2000 and a J&M TIDAS spectrometer, were used. In case of a monochromatic source a photo diode was employed as detector. The given sample-detector separation does not detect light scattered with an angle greater than 0.4°. The small amount of unwanted scattered light measured within the cone of 0.4° is negligible.

To avoid the influence of multiple scattered light on the measurement either the sample can be diluted or the thickness of the cuvette can be decreased. In this study the fat emulsion are diluted with distilled water to a fat concentration of less than 0.05% which is low enough to avoid the influence of multiple scattered light.

2.2. Spatially resolved reflectance setup

A spatially resolved reflectance setup is applied to measure the light intensity $R(r)$ emitted by a semi-infinite sample which is illuminated perpendicular with a collimated point source. In this work it was employed to measure the reduced scattering coefficient of diluted fat emulsion samples. The spatial resolved reflectance $R(r)$ of homogeneous, semi infinite media can be calculated with the diffusion Eqs. [13, 14]. The diffusion equation is a simplification of the more precise transport theory. The diffusion equation supplies a good correlation to measurements with the following constraints. The distance to the source has to be large, $r >> 1/\mu_s'$, and the medium has to be highly scattering, $\mu_s' >> \mu_a$. For unknown absorption and scattering properties of the media, an inverse calculation of the diffusion equation was employed to calculate the absorption and scattering coefficients of the sample. In general, the diffusion equation is fitted to the measured spatially resolved reflectance $R(r)$ with variable μ_a, μ_s' and a multiplicative adjustment variable.

The absorption of the diluted samples is mainly given trough water absorption for wavelength longer than 550 nm, see section 3.5. The fat emulsions were diluted to roughly 0.5 Vol-% fat concentration for the measurement of the spatially resolved reflectance. With the known absorption coefficient, the inverse calculation has only 2 fitting parameters, μ_s' and the multiplicative factor, thus the reduced scattering coefficient can be calculated with high accuracy.

A CCD-camera based setup was employed, as can be seen in Fig. 2(a). Either a tuneable 5 color He-Ne laser or a xenon-lamp monochromator source was used to illuminate the sample. In comparison to the diffusion equation which computes the spatially resolved reflectance for perpendicular illumination with an infinitesimal small point source our measurement setup exhibits some differences. As can be seen in Fig. 2(a), the sample was not illuminated perpendicular and the Xe-monochromator light source has a small numerical aperture (NA) and a spot diameter of roughly one mm on the sample. As calibration measurements and simulations show, the angle of incidence of the light source as well as the spot diameter and divergence of the light sources are negligible for samples with optical properties like we used in this study.

The accuracy of the inverse calculation of μ_s' was analyzed with Monte Carlo simulations. The inverse calculation with known μ_a produced errors of less than 1 % for Monte Carlo simulations using Henyey Greenstein phase function with μ_a, μ_s and g similar to the optical properties of the measurements. Monte Carlo simulations which were performed with the measured phase function of Lipovenoes 10 % instead of the Henyey-Greenstein phase function produced higher errors which are still below 3%. An illustration to the difference of Henyey Greenstein and Lipovenoes phase functions with the same g factor is given in Fig. 3(b).

As reported previously [15], a CCD camera based spatially resolved reflectance setup is affected by errors due to scattered and reflected light inside the objective. The measurements can be corrected by deconvoluting the objective point spread function. This point spread func-

#92339 - $15.00 USD Received 1 Feb 2008; revised 18 Mar 2008; accepted 4 Apr 2008; published 11 Apr 2008
(C) 2008 OSA

tion has to be measured for each wavelength and camera setup individually. This is very time consuming and was not feasible for this study but the error of the camera objective is small for optical properties like those measured here. The error will raise for higher values of μ_a or μ_s' because the dynamic range of the spatially resolved reflectance function $R(r)$ will raise. The errors that are expected for a CCD based measurement setup were investigated with convoluted Monte Carlo simulations. The previous Monte Carlo simulation which utilizes the phase function of Lipovenoes 10 % was convoluted with the point spread function of the camera objective which was measured at 633 nm. The inverse calculation of the convoluted simulation showed a deviation of up to 8 %. Thus the inverse calculation of the measured spatially resolved reflectance is expected to have an uncertainty of about 8% for samples with similar optical properties.

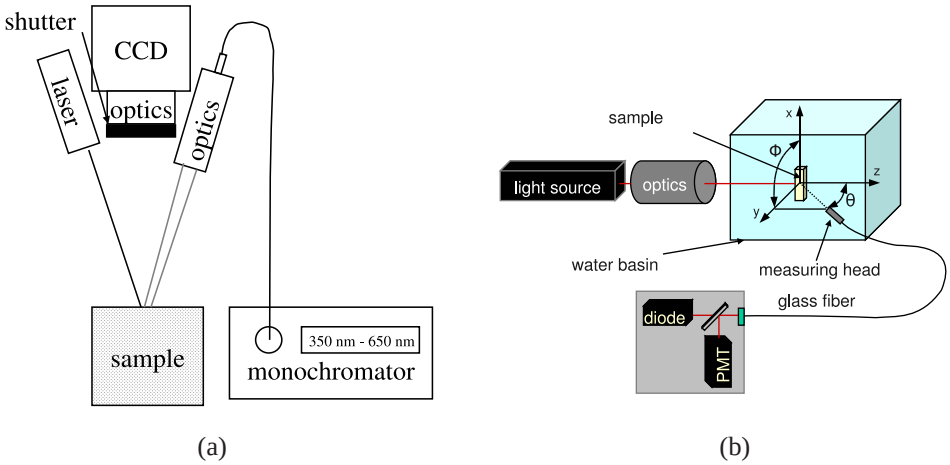

Fig. 2. a) Scheme of the CCD based spatially resolved reflectance setup to measure the reduced scattering coefficient. The sample is illuminated either with a laser or a collimated xenon-lamp monochromator source. b) Sketch of the goniometric setup to measure the phase function in the whole solid angle and thus the *g* factor.

2.3. Goniometer setup

According to the transport theory turbid media are sufficiently defined through their absorption and scattering coefficients and their phase function. The phase function $p(\vec{s},\vec{s}')$ describes the probability that a photon having an incident direction $\vec{s}$ is scattered in direction $\vec{s}'$, see Fig. 3(a). The phase functions of different scattering samples can vary strongly. Also phase functions with the same anisotropy factor can have big differences, see Fig. 3(b).

The goniometric setup is used to measure the phase function of a scattering media. As can be seen in Fig. 2(b), the scattering sample is illuminated in z direction with a collimated light source and the angle dependent scattering intensity $p(\theta,\phi)$ is measured for nearly the whole solid angle [16, 17]. By tilting the sample it is possible to measure the phase function $p(\vec{s},\vec{s}')$ for many incident directions $\vec{s}$. However, for spherical scatterers like fat droplets the phase function is independent of the incident direction $\vec{s}$ and can be noted as $p(\theta,\phi)$. Furthermore the phase function is rotationally symmetric for unpolarized light. That means, the phase function $p(\theta)$ is constant for different ϕ. With our setup the phase function $p(\theta)$ of spherical scatterers is always measured in the z-y plane. The polarization direction of an incident linear polarized light source is rotated using special optics. The phase function of the whole solid angle $p(\theta,\phi)$ can be calculated by the superposition of the phase function for perpendicular (in respect to

#92339 - $15.00 USD Received 1 Feb 2008; revised 18 Mar 2008; accepted 4 Apr 2008; published 11 Apr 2008
(C) 2008 OSA

the measurement plane) (p_{per}) and parallel (p_{par}) polarized light $p(\theta,\phi) = p_{per}(\theta)\cdot\cos(\phi) + p_{par}(\theta)\cdot\sin(\phi)$.

The employed goniometric setup holds some special features. The scattering sample was held inside an index matching tank, filled with distilled water. This minimizes the total internal reflection and also the refraction of scattered light exiting the sample. A collimated J & M Xe-lamp monochromator was used as light source. The numerical aperture (NA) of the incident light was adapted to the NA of the detection fiber. The Xe-monochromator emits light from 280 nm to 650 nm with a spectral bandwidth of roughly 10 nm. The scattered light was collected by a 600 µm multimode glass fiber with a fiber-sample distance of 8 cm.

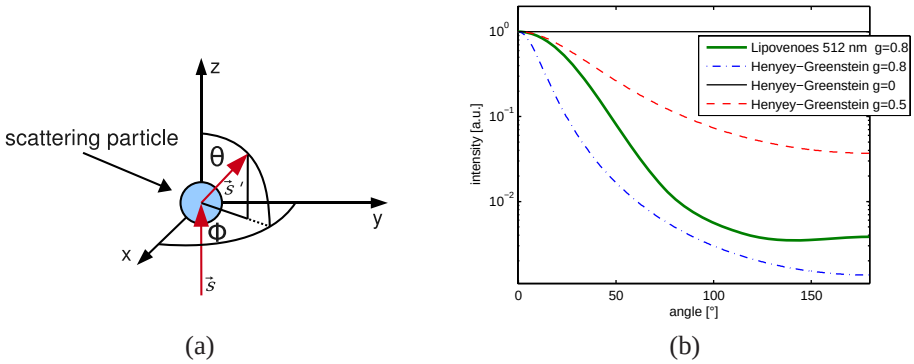

(a) (b)

Fig. 3. a) Scheme of the coordinate system which is used for the phase function measurements. The scattering particle or the sample is illuminated from direction $\vec{s}$. The scattering occurs in direction $\vec{s}'$. The incident direction of our measurements $\vec{s}$ was in z direction. For rotational symmetric scatterers the scattering of unpolarized light is independent of ϕ. b) Plot of different phase functions. The commonly used Henyey Greenstein phase function can be adjusted with the g parameter to isotropic scattering (g=0) forward scattering (g>0) and backward scattering (g<0). The g parameter of the Henyey Greenstein phase function is identical to the anisotropy factor g, the averaged cosine over all angles. As comparison the phase function of Lipovenoes 10% ($\lambda = 512$nm, unpolarized), which has an anisotropy factor of g =0.8 is plotted (green). Please note the large difference between the Lipovenoes-, and the Henyey Greenstein phase function despite their identical anisotropy factor.

The NA of the detection fiber was reduced with a pinhole in front of the fiber (⌀= 1 mm, distance to the fiber = 5 mm). This minimizes the detection of multiple scattered light which exits the sample far from the incident beam. A computer controlled 2 axes step motor driven arm moved the fiber. The minimum possible step width was 0.25°. The light which was collected by the fiber was directed with a multiplexer either to a photodiode or to a photomultiplier. This results in a measurement range of about 12 orders of magnitude of light intensity.

2.4. Phase function correction

Many groups have used cylindrical cuvettes [6] for the goniometric measurement of liquid samples like Intralipid. Cylindrical cuvettes admit the measurement of the phase function $p(\theta)$ for all $\theta-$angles. Slab geometry cuvettes, like the ones used in this work, prohibit the measurement of the phase function in slab direction (usually the x-y plane). Since this goniometer is originally built to measure thin slices of biological samples, correction algorithms for samples in slab geometry have been developed. Hence, a slab geometry cuvette was used for the measurement of the fat emulsions as is shown in Fig. 4(a). We note that the distortion of the

#92339 - $15.00 USD Received 1 Feb 2008; revised 18 Mar 2008; accepted 4 Apr 2008; published 11 Apr 2008
(C) 2008 OSA

phase function measurement caused by a cylindrical cuvette is not that obvious, but it has to be corrected similar as it is done for slab geometry cuvettes. Furthermore, cylindrical cuvettes produce a strong distortion of the incident beam, thus they appeared unsuitable for phase function measurement with high angle resolution in our opinion.

The most obvious distortion caused by the slab geometry cuvette to the phase function is the increasing Fresnel reflection of scattered light for angles of θ toward 90°. As can be seen in Fig. 4(b), no light is exiting the cuvette at $\theta = 90°$ (dashed line). Furthermore, the incident beam is reflected at the rear glass which causes the phase function to be superposed by itself in backward direction. Also, the scattered light itself is reflected at the glass/fluid boundary when exiting the cuvette. An analytical solution for the correction of these distortions was developed. The forward calculation of the distortion and the backward correction are shown in Fig. 4(b) for a theoretical phase function of Intralipid. The geometrical errors can be corrected completely if single scattering is assumed.

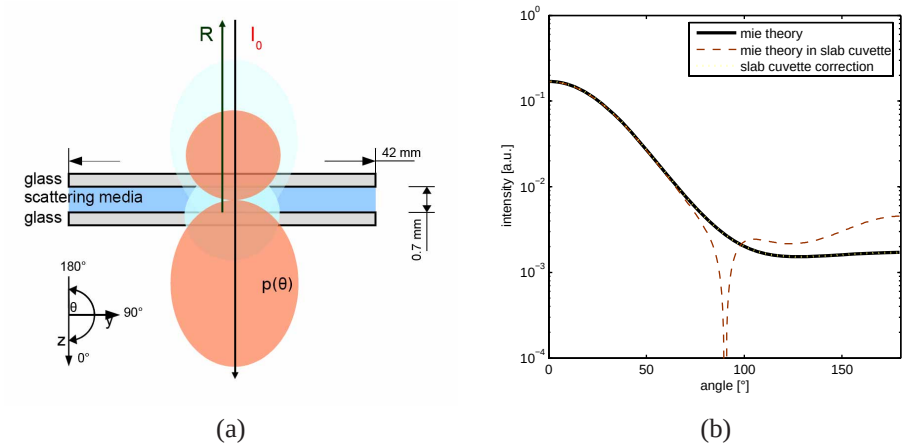

Fig. 4. a) Sketch of the cuvette geometry. The scattering sample is held inside two glass slides. Usually the cuvette is parallel to the x-y plane. The principal distortions that influence the measured phase function are shown. The incident laser beam I_0 is reflected at the back of the cuvette. The reflected intensity R causes scattering in the opposite direction. Also the scattered light itself (red) is reflected at the glass boundaries (blue). Both effects produce the distortion of the phase function which can be seen in the plot on the right. In x-y plane, $p(\theta) = 90$, the light cannot exit the cuvette. b) The theoretical phase function of Intralipid was calculated according to van Staveren [5] (solid line). The distortion due to the cuvette was calculated for this phase function (dashed line). The characteristic distortion at 90° and in backward direction can be seen. The backward correction (dotted line) shows no deviation to the theory.

The correction algorithm was also applied for tilted irradiation. Then $\vec{s}$ is still in z direction, but the cuvette is rotated around the x axis and has an angle to the x-y plane. This is demonstrated in Fig. 5. Figure 5(a) shows the measurement of Lipovenoes 20 % in a cuvette having slab geometry with different angles of the cuvette to the x-y plane. It was illuminated with perpendicular (in respect to the measurement plane) polarized light at $\lambda = 650\,\text{nm}$. The measurement was performed for tilt angles of the cuvette of 0°, 9.3°, 16.8° and 33.3° (respective to the x-y plane). The distortion of the phase function depends on the tilt angle. The shading of the cuvette moves from 90° toward 56.7°. Additionally, the reflected peak of the incident beam moves from 180° toward 113.4°.

#92339 - $15.00 USD Received 1 Feb 2008; revised 18 Mar 2008; accepted 4 Apr 2008; published 11 Apr 2008
(C) 2008 OSA

In Fig. 5(b) these measurements are corrected for the geometrical distortion. The corrected measurements show a good correlation to each other. The correction due to the cuvette shows discrepancies only in cuvette direction which can be explained by multiple scattering. By measuring the phase function with several tilt angles of the incident beam it is possible to reconstruct a continuous phase function from 10°-165°. For angles smaller than 10° the phase function is superposed with the unscattered incident beam. For angles larger than 165° the incident beam is blocked by the detector itself. With a method we already have presented [17] it was possible to reconstruct the missing parts of the phase function. With the knowledge of the phase function for the whole solid angle the g-factor can be calculated as it is explained in section 2.6. With the known anisotropy factor it is possible to compare the measurement of the collimated transmission and the spatially resolved reflectance using

$$\mu_s' = \mu_s(1-g). \tag{2}$$

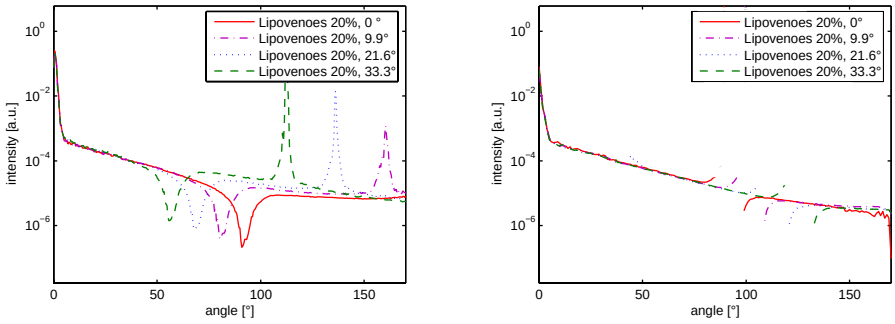

(a) (b)

Fig. 5. a) Plot of the measured phase function of Lipovenoes 20 % ($\lambda = 650$ nm, perpendicular polarization) inside a slab geometry cuvette for different tilt angles of the cuvette to the x-y plane. The distortion of the phase function depends strongly on the angle of irradiation. b) Plot of the corrected phase functions of the measurements from (a).

2.5. Fat emulsions

Fat emulsions consist mainly of soy bean oil, water, glycerin, and egg lipid. The manufacturers add different additional components in unknown quantities for pH adjustment and stabilization of the fat emulsions. Also the quantity of soy bean oil and glycerin vary by brand and concentration. The samples which were measured in this study are listed in Tab. 1.

The scattering properties, μ_s, μ_s', g and $p(\theta)$, of the fat emulsions can be calculated with Mie theory, as it is explained in section 2.6. For the calculation with Mie theory the knowledge of the size distribution of the fat droplets, the inner and outer refractive index of the fat droplets as well as the volume concentration of the droplets are needed.

Glycerin is dissolved in water which raises the refractive index insignificantly by 0.17 %. The water-glycerin mixture as well as the soy bean oil do not inherently scatter light. When the soy bean oil is mixed with the water-glycerin and emulsified with egg lipid, the oil is suspended in water inside small droplets with a monolayer lipid membrane. The small oil droplets cause the scattering in the emulsion. The volume concentration of the scattering particles was measured by centrifuging the samples, which separates a clear fluid from a stiff cream layer. After

#92339 - $15.00 USD Received 1 Feb 2008; revised 18 Mar 2008; accepted 4 Apr 2008; published 11 Apr 2008
(C) 2008 OSA

separating the cream layer from its water residuals, the remaining mass equaled the sum of egg lipid and soy bean oil. This testifies that the scatterers are formed only by soy bean oil and egg lipid as can be seen in Fig. 6(a). The density of soy bean oil is approximately 0.927 g/ml [18] at 20°C, the density of egg lipid could not be measured precisely in our lab but it is close to 1 g/ml at 20°C.

Tab. 1. Ingredients of the investigated fat emulsions. Lipovenoes and Intralipid is fabricated by Fresenius Kabi, ClinOleic is fabricated by Baxter.

g / liter	Lipovenoes 10%	Lipovenoes 20%	ClinOleic 20%	Intralipid 10%	Intralipid 20%	Intralipid 30%
Soybean oil	100	200	160	100	200	300
Olive oil	0	0	40	0	0	0
Glycerol	25	25	22.5	22	22	16.7
Eggphospholipid	6	12	0	12	12	12
Elicitin	0	0	12	0	0	0
Sodium oleat	included	included	0.3	0	0	0
Sodium hyd.	included	included	included	included	included	included
pH-Value	6.5-8.7	6.5-8.7	6-8	8	8	8

Fat emulsions consist of more egg lipid than is needed to encapsulate the soy bean oil. The rest of the egg lipid builds up small micelles. The manufacturer controls the maximum size of the fat droplets. Fat droplets which are bigger than a few µm could cause thrombosis in small vessels [19]. Fat emulsions have a broad particle size distribution. The size distribution of Intralipid 10 % is known from previous publications [5]. The smallest particles are micelles of egg lipid of only a few nm diameter. The biggest particles are fat droplets which are slightly smaller than 1 µm in diameter. The particles in the fat emulsions are very stable. If a sample is stored for a while, it may happen that the fat droplets are concentrated in the top and a gradient of scattering can be seen (more scattering at the top). After mixing it again there is no observable change in scattering attributes. Also dilution of the fat emulsion with water is not changing the size distribution of the particles.

The refractive index of water is known precisely. One formulation is provided by the IAPWS [20] which gives the refractive index over a broad range of wavelengths, pressure and temperature conditions. The Cauchy equation [18] is sufficient for the calculation of the refractive index of water at room temperature for NIR and VIS wavelengths, see Eq. 3. It is not valid for wavelengths below 400 nm and is showing deviations to the more precise IAPWS method

$$n(\lambda) = I + J/\lambda^2 + K/\lambda^4, \tag{3}$$

with $I_{water} = 1.311$, J=1.154×10^4 and K=-1.132×10^9. The wavelength λ is given in nanometers. The wavelength dependent refractive index of soy bean oil is not well-investigated. Van Staveren, et al., [5] used the Cauchy equation with $I_{soy} = 1.451$ and the same J and K coefficients that are used for water. Thus, soy bean oil is expected to show the same dispersion as water with a constant difference of $\Delta n = n_{soy} - n_{water} = I_{soy} - I_{water} = 0.140$. We performed refractometer measurements which did not show differences outside the measurement accuracy to $n(\lambda)_{soy}$ calculated with Eq. 3 for wavelength higher than 400 nm. For wavelengths below 400 nm the results of Eq. 3 are invalid. Mie theory can be used slightly below 400 nm because the refractive index difference between soy bean oil and water, Δn, is expected to be constant. The refractive index of egg lipid is not known and is assumed to be identical to the refractive index of soy bean oil. For ClinOleic the refractive index of olive oil is assumed to be identical with soy bean oil.

#92339 - $15.00 USD Received 1 Feb 2008; revised 18 Mar 2008; accepted 4 Apr 2008; published 11 Apr 2008
(C) 2008 OSA

2.6. Mie theory

With the known particle size distribution and the refractive index of the particles and the volume concentration, it is possible to calculate the optical properties, μ_s, μ_s', g and the phase function $p(\theta)$, of the fat emulsions using Mie theory. The Mie theory is the analytical solution of the Maxwell's equations for the scattering of electromagnetic wave by a single spherical particle [21]. To calculate the optical properties of a suspension of different particle sizes it is important that the particles are independently scattering. The independent scattering approximation is valid for interparticle distances which are longer than the wavelength. This condition is valid for fat emulsions with scatterer concentration less than 4 Vol-% [12, 10].

On that condition separate Mie theory calculations can be employed for the different particle diameters d found in the solution. The scattering coefficient of the solution can be calculated with

$$\mu_s = \sum_d \frac{C_{sca}(d) \cdot \sigma_{sca}(d)}{V(d)}. \tag{4}$$

μ_s equals the sum of the scattering cross sections C_{sca}, which is calculated with Mie theory, for every particle diameter weighted by the volume concentration σ_{sca} (volume of fat and egg lipid divided by the total volume) and particle volume $V(d) = \frac{4}{3}\pi(d/2)^3$.

The phase function of the whole solution is calculated analogous to Eq. 4. For every particle diameter d a single phase function $p_i(\theta)$ can be calculated using Mie theory. The phase function of the whole solution $p_{tot}(\theta)$ is the sum of all, unnormalized, $p_i(\theta)$ weighted by the number of particles N_i with the corresponding diameter

$$p_{tot}(\theta) = \sum_i \frac{N_i \cdot p_i(\theta)}{N_{tot}}, \tag{5}$$

with the total number of particles, $N_{tot} = \sum N_i$. With the knowledge of the phase function the anisotropy factor g is determined by

$$g = \frac{\int_{4\pi} p(\Omega)\cos\theta d\Omega}{\int_{4\pi} p(\Omega) d\Omega}. \tag{6}$$

2.7. Size distribution calculation

Van Staveren, et al., measured the size distribution of Intralipid 10 % using electron microscopy as can be seen in Fig. 6(b) (crosses). The direct measurement of the particle size distribution of fat emulsions with an electron microscope is complicated and was not feasible in this study.

We calculated the size distribution of the fat emulsions on the basis of our measurement data. For each fat emulsion we performed measurements of the phase function for wavelengths from 350 nm to 650 nm and the scattering coefficient for wavelengths from 400 nm to 900 nm. These measurement data were fitted to a Mie theory calculation of a suspension with unknown size distribution. A size distribution of each fat emulsion is calculated which fits the measured μ_s and the phase function for all measured wavelengths. A Gaussian distribution of particle sizes did not fit the measurements. The attempt to fit a free size distribution did not succeed. The size distribution of Intralipid 10 % which was measured by van Staveren [5] shows a linear decay in logarithmical scale towards bigger particles. Thus we assumed a size distribution with a linear decay in logarithmical scale for all fat emulsions. This assumption leads to the following relation,

$$N(d) = 10^{\alpha \cdot d},\ d \in [d_{min}, d_{max}]. \tag{7}$$

Equation 7 describes the size distribution $N(d)$ of fat emulsions with only two parameters, the constant decay α and the maximum particle size d_{max}. The number of particles $N(d)$ is

#92339 - $15.00 USD Received 1 Feb 2008; revised 18 Mar 2008; accepted 4 Apr 2008; published 11 Apr 2008
(C) 2008 OSA

calculated for every particle diameter d from the minimum diameter d_{min} to the maximum diameter d_{max}. The smallest particles in fat emulsions are lipid micelles. A minimum micelles diameter of $d_{min} = 25\,\text{nm}$ is assumed. The maximum diameter d_{max} can differ in dependence of the manufacturing process, thus it was a free fitting parameter. For the Mie theory calculation 21 discrete values of d between d_{min} and d_{max} are used.

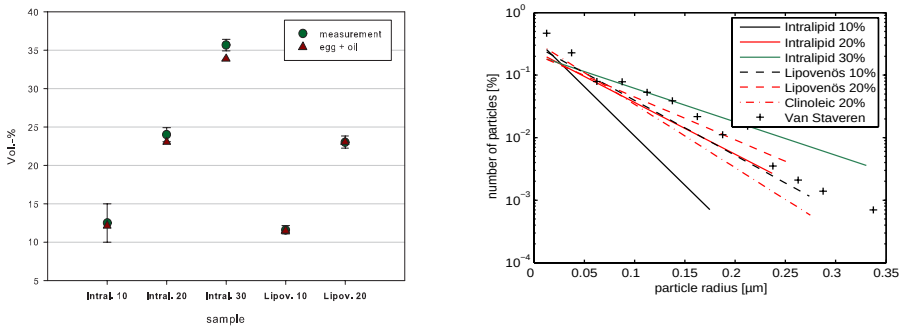

(a) (b)

Fig. 6. a) Plot of the measured scatterer concentration in different fat emulsions (green dots). The measurements match the Vol-% concentration of scatterers (red triangles) which was calculated from the contained soybean oil and egg lipid. b) Plot of the particle size distribution of the different fat emulsions which are used for the Mie theory calculations.

With Eq. 7 it is possible to fit the size distribution to the measurement results. Therefor the size distribution was fitted with Mie theory to the whole phase function for 650 nm (except inaccessible parts) and the measured scattering coefficient for 650 nm. The calculated size distributions of all fat emulsions can be seen in the Fig. 6(b), the values of the two fitting parameters, α and d_{max}, are listed in Tab. 2.

Tab. 2. Coefficients for the calculation of the particle size distribution with Eq. 7 for different fat emulsions.

	Lipovenoes 10%	*Lipovenoes* 20%	*ClinOleic* 20%	*Intralipid* 10%	*Intralipid* 20%	*Intralipid* 30%
$\alpha[m^{-1}]$	-4.4086e6	-3.429e6	-5.074e6	-7.884e6	-4.151e6	-2.679e6
$d_{max}[m]$	0.5477e-6	0.5133e-6	0.5494e-6	0.3497e-6	0.4739e-6	0.6607e-6

We note that the optical parameters calculated with Mie theory for the size distribution originally measured by van Staveren [5] show no significant difference to the calculation with a size distribution which was approximated to his measurement results and obeys to Eq. 7.

3. Results

The direct measurements of μ_s, μ_s', g and $p(\theta)$ of six different fat emulsions within a wavelength range from 400 nm to 900 nm are presented. Additionally, the optical properties are calculated with the Mie theory method which was explained in section 2.6 and the calculated size distribution of section 2.7. Finally simple equations are provided for the calculation of the optical properties of each measured fat emulsion for wavelengths from 400 nm to 1000 nm for unpolarized light.

#92339 - $15.00 USD Received 1 Feb 2008; revised 18 Mar 2008; accepted 4 Apr 2008; published 11 Apr 2008
(C) 2008 OSA

3.1. *Phase function*

Since it would exceed the scope of this paper we cannot plot phase functions for 6 different samples, for parallel and perpendicular polarized light and for wavelenghts from 350 to 650 nm. We concentrate on the discussion of the phase functions of 2 samples for 350 to 650 nm. In Fig. 7 the phase function of Lipovenoes 10 % and Intralipid 20 % was calculated with Mie theory using the derived particle distribution. The calculated phase functions are plotted against the corresponding measurements. The calculations are forward corrected for the slab geometry cuvette. The calculations show a good correlation with the measured phase function apart from regions which could not be measured. For shorter wavelengths deviations around 120° can be seen.

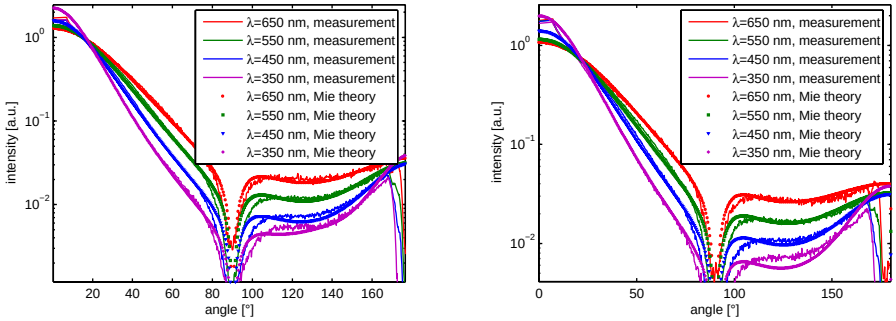

Fig. 7. Comparison of the phase function calculated with Mie theory to the phase function measurement for 2 different samples and 4 different wavelengths. The goniometric measurement is not corrected for distortions of the glass cuvette, but the Mie Theory calculation is forward corrected for a phase function measurement inside a glass cuvette. a) Comparison for Intralipid 20 %, b) Comparison for Lipovenoes 10 %.

The deviation at 120° can be explained using the Monte Carlo method. Monte Carlo simulations were performed which accounted for the measurement setup considering the glass cuvette, see Fig. 8. The phase functions calculated for Lipovenoes 10 % for 350 nm and 650 nm are used for the simulations. One for a very low concentrated sample (green curve) with less than 0.004 Vol-% scatterer concentration and one for a sample with scatterer concentration of 0.04 Vol-% which is similar to the volume concentration used for goniometric measurements (red curve).

The low concentration simulation is close to the theoretical values. The higher concentration simulation matches the measurement results and shows similar deviations to the theory for short wavelengths as the measurements do. It can be stated that these deviations around 120° are generated through multiple scattering inside the cuvette. This effect can mainly be observed at short wavelengths because the decay of the phase function is higher for shorter wavelengths. Unfortunately, it was not possible to decrease the sample concentration to avoid multiple scattering because the small light intensity of the xenon-lamp monochromator forced us to balance signal to noise ratio with measurement variables like the sample concentration.

With the help of the Monte Carlo simulation it is possible to calculate the systematic error which the multiple scattering adds to the determination of the g factor. For 650 nm the g factor is not significantly affected, for 350 nm, the measured g factor is lowered by 3 %. From 650 nm to 350 nm we expect, according to our experience, a linear increase of the error. The g factor measurements presented in section 3.2 are corrected for these errors.

#92339 - $15.00 USD Received 1 Feb 2008; revised 18 Mar 2008; accepted 4 Apr 2008; published 11 Apr 2008
(C) 2008 OSA

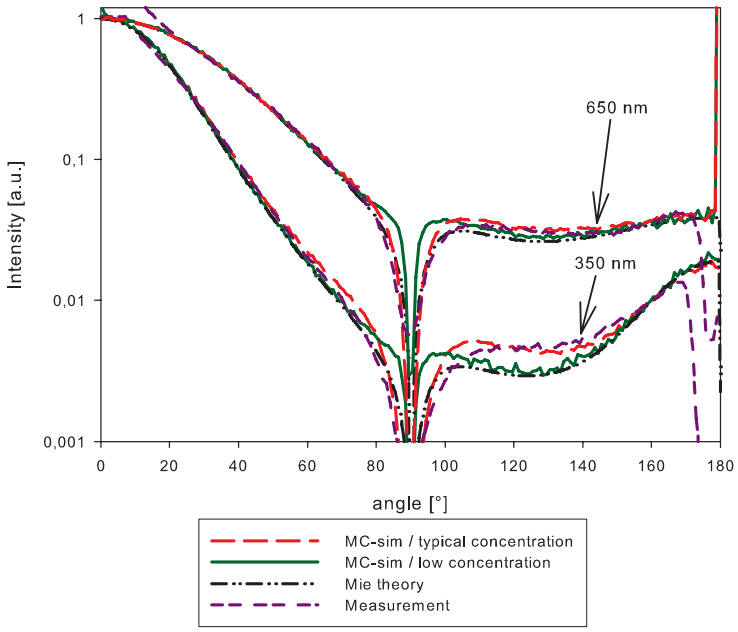

Fig. 8. Plot of the phase function of Lipovenoes 10 % for 350 nm and 650 nm. The comparison between the measurement results (purple curve), Mie theory (black curve) and Monte Carlo (MC) simulations for two different concentrations are shown. One MC simulation is calculated with a low concentration of scatterers inside the cuvette (0.004 Vol-%, green curve), the other is calculated for a concentration of scatterers similar to the measurement setup (0.04 Vol-%, red curve). The measurement and the Monte Carlo simulation with higher concentration show a deviation from the theory at 120° for short wavelengths.

3.2. Anisotropy factor

After correction and reconstruction of the measurement data as described in section 2.4 the anisotropy factor g was calculated, see Fig. 9. The measured anisotropy factors were corrected for multiple scattering at small wavelengths as it is explained in the end of section 3.1. In Fig. 9 the measured anisotropy factor is plotted for the six different fat emulsions for non polarized light from 350 nm to 650 nm. The corresponding Mie theory calculations for the different size distribution of the according samples are shown. The measurements show a good correlation with the Mie theory calculations. The anisotropy factor is strongly dependent on the wavelength. Large differences between the different samples are found. The relative standard deviation of the measured g is less than 1 % and, thus, within the symbol sizes. It was calculated from multiple measurements using different bottles of the same brand. The measured anisotropy factors of the samples exhibit large deviations to the anisotropy factor reported by van Staveren [5] for Intralipid 10%.

#92339 - $15.00 USD Received 1 Feb 2008; revised 18 Mar 2008; accepted 4 Apr 2008; published 11 Apr 2008
(C) 2008 OSA

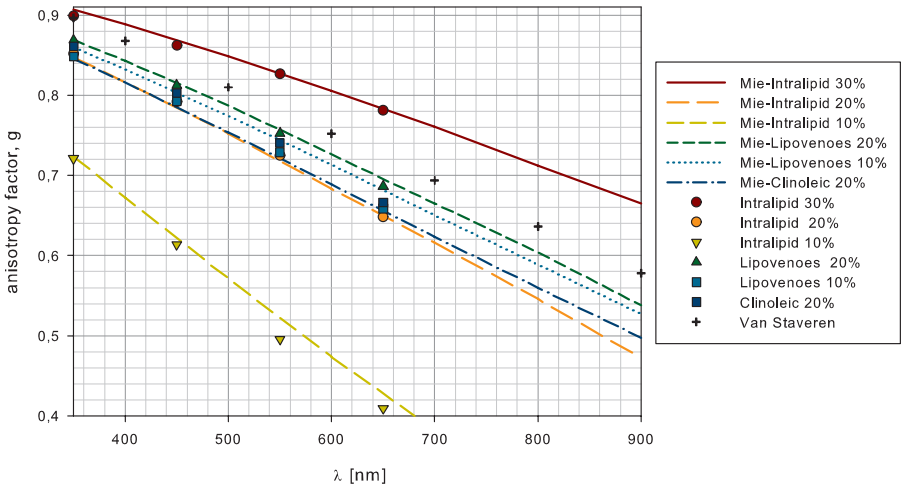

Fig. 9. Plot of the anisotropy factor of different fat emulsions vs. wavelength from $\lambda = 350\,\text{nm} - 650\,\text{nm}$ measured with the goniometric setup (symbols). The corresponding calculations with Mie theory are plotted in the same color (curves).

3.3. *Scattering coefficient*

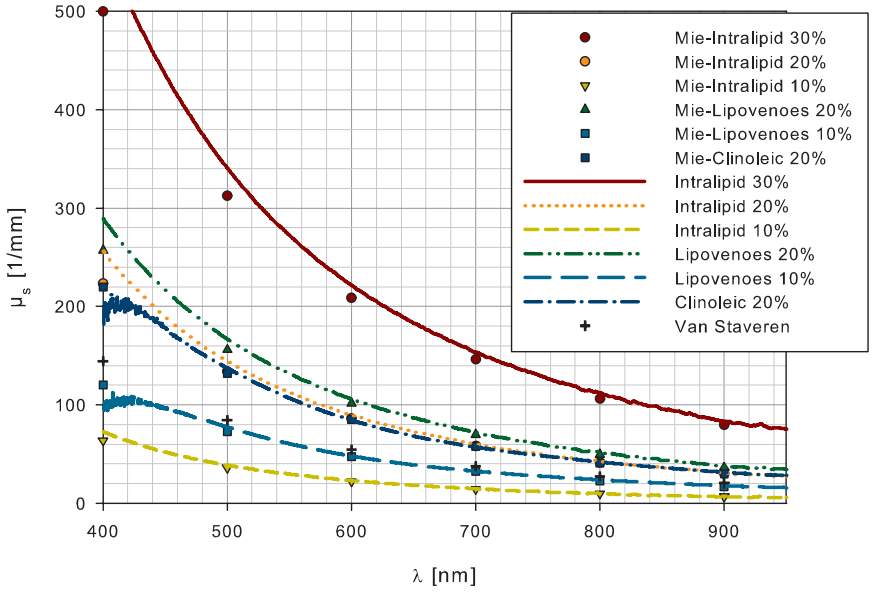

Fig. 10. Plot of the scattering coefficient (scaled for undiluted samples) versus the wavelength for the different fat emulsions, measured with the collimated transmission (curves). The corresponding calculations with Mie theory are plotted in the same color (symbols).

The results for the scattering coefficient μ_s of the different fat emulsions measured with the collimated transmission setup are plotted from 400 nm - 900 nm in Fig. 10. The results are given for

#92339 - $15.00 USD Received 1 Feb 2008; revised 18 Mar 2008; accepted 4 Apr 2008; published 11 Apr 2008
(C) 2008 OSA

the undiluted fat emulsions. The relative error of μ_s is approximately 3% for all wavelengths. It was calculated from multiple measurements of nine different bottles of Lipovenoes 20%. The Mie theory calculations are plotted in the same color as the corresponding measurements. The relative difference between theory and measurement reaches its maximum of about 10% for small wavelengths. The differences of the various samples are large in comparison to the standard deviation of different measurements on the same sample.

3.4. Reduced Scattering Coefficient

Measurements of the reduced scattering coefficient were performed with the spatially resolved reflectance setup. The results are shown in Fig. 11. Each sample except ClinOleic 20% was measured with a multicolor He-Ne at 543 nm, 594 nm, 612 nm and 633 nm. Lipovenoes 10% and Lipovenoes 20% are measured additionally with a Xe-monochromator setup for wavelengths from 400 nm to 650 nm. The reduced scattering coefficient was also calculated with Mie theory calculations of μ_s and g, with $\mu_s' = (1-g)\mu_s$. The differences of the measurements compared to the theory can be explained by the error analysis of this method which is explained in section 2.2. In contrast to the preceding measurements of μ_s and g the measured reduced scattering coefficient of Intralipid 10% (and Lipovenoes 10%) is close to the values measured by van Staveren [5]. Interestingly, the significant differences in g and μ_s of Intralipid 10% do accurately compensate one another [22]. Also the fat emulsions with higher scatterer concentration would have a reduced scattering coefficient similar to van Staveren's measurements, when diluted to the scatterer concentration of Intralipid 10%.

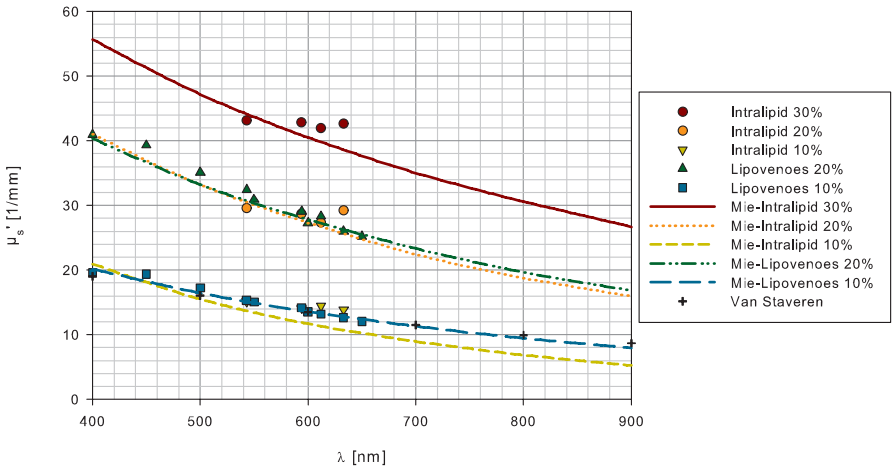

Fig. 11. Plot of the measured reduced scattering coefficient (scaled for undiluted samples) for the different fat emulsions for wavelengths from 400 nm to 650 nm (symbols). The corresponding calculations with Mie theory are plotted in the same color (curves).

3.5. Absorption coefficient

The absorption coefficient of a fat emulsion is calculated by the sum of the absorption coefficients of its ingredients. Fat emulsions are low absorbing at visible wavelengths. The predominant absorbers are soy bean oil and water. The absorption of glycerin and egg lipid can be ignored due to the low concentration. The water absorption is well known from literature [23]. A soy bean oil sample from Fresenius Kabi was measured. The absorption of soy bean oil

#92339 - $15.00 USD Received 1 Feb 2008; revised 18 Mar 2008; accepted 4 Apr 2008; published 11 Apr 2008
(C) 2008 OSA

is small for VIS wavelengths higher than 500 nm ($\mu_a(VIS) \leq 0.001\,\mathrm{mm}^{-1}$). The absorption is strongly increasing versus smaller wavelengths, as can be seen in Fig. 12.

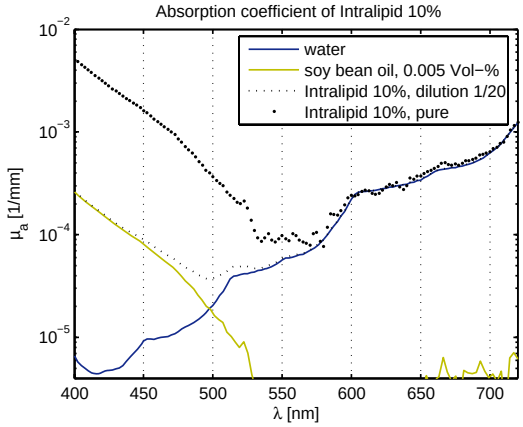

Fig. 12. Plot of the absorption coefficient of Intralipid 10 %. The absorption of the solution is combined from the absorption of water and soy bean oil. When Intralipid 10 % is diluted to 0.5 Vol-% scatterer concentration, the absorption of soy bean oil is negligible for wavelengths higher than 550 nm.

The total absorption of a fat emulsions, $\mu_{a(ges)}$, is the sum of the single absorbers multiplied with their volume concentration

$$\mu_{a(ges)} = \sum_{i=1}^{n} \mu_{a(i)} \cdot \sigma_{sca(i)}. \tag{8}$$

For fat concentrations like they were used for the measurement of the spatially resolved reflectance (typically below 0.5 Vol-%) the soy bean oil absorption is negligible for wavelengths longer than 550 nm, as can be seen in Fig. 12.

3.6. Fitted equations

To give an easy access to the above shown results simple equations to calculate the optical properties of the fat emulsions are provided. We found that the anisotropy factor $g(\lambda)$ can be approximated by a linear function

$$g(\lambda) = y_0 + a \cdot \lambda, \tag{9}$$

the scattering coefficient $\mu_s(\lambda)$ by a power function

$$\mu_s(\lambda) = a \cdot \lambda^b \tag{10}$$

and the reduced scattering coefficient $\mu_s'(\lambda)$ by a polynomial of second order

$$\mu_s'(\lambda) = y_o + a \cdot \lambda + b \cdot \lambda^2. \tag{11}$$

The Eqs. 9-11 are fitted to the Mie theory calculations from 400 nm to 900 nm. The corresponding parameters for the calculation of the optical properties of the different fat emulsions are listed in Tab. 3, 4 and 5 in the appendix. For the coefficients given in the tables, the wavelength has to be given in [nm] (e.g. λ=650 for red light), then μ_s and μ_s' of the undiluted fat emulsions are obtained in [mm^{-1}] .

#92339 - $15.00 USD Received 1 Feb 2008; revised 18 Mar 2008; accepted 4 Apr 2008; published 11 Apr 2008
(C) 2008 OSA

Also the absorption coefficient was approximated with a simple equation. The absorption coefficient measurements of soy bean oil and water were fitted from 380 nm - 780 nm to a sigmoid function. The parameters for the calculation of $\mu_a(\lambda)$ of pure water and soy bean oil are listed in Tab. 6 in the appendix. The absorption coefficient is obtained in [mm^{-1}] for the pure substance with

$$\mu_a(\lambda) = a/\left(1+e^{-\frac{\lambda-x_0}{b}}\right). \tag{12}$$

The soy bean oil absorption coefficient is sufficiently described by Eq. 12. The calculation of the water absorption with Eq. 12 is only a convenient approximation. More precise values for the water absorption are available in literature [23]. The errors which are added to the optical properties with the fitting algorithms can be estimated with the residual which is given beside the parameters in the appendix. The residual r^2 is defined by $r^2 = 1 - S_{err}/S_{mean}$ with S_{err}, the sum of squares error and S_{mean} the sum of squares about the mean. A perfect fit is characterized by a residual of one, in practice a good fit is characterized by a residual very close to one (e.g. 0.99 or 0.999).

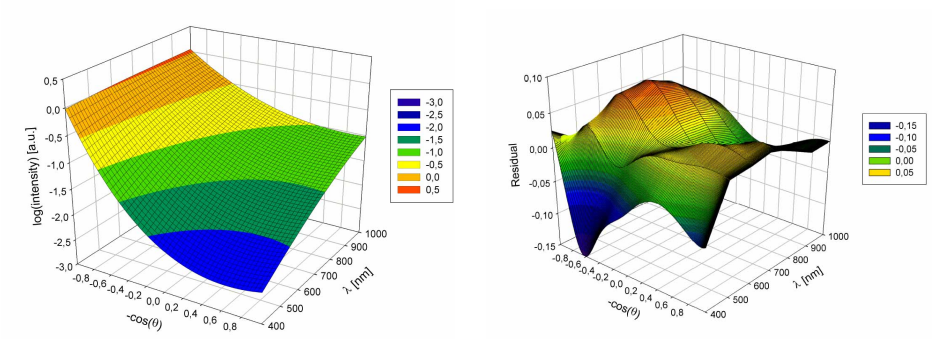

(a) (b)

Fig. 13. a) Plot of the phase function of ClinOleic 20% for wavelengths from 400 nm to 1000 nm. The logarithm of the Intensity $I(\lambda,\theta)$is plotted over the negative cosine of θ for angles from 0° to 180°. b) Plot of the absolute difference of the surface fit to the data of (a).

In order to find an analytical expression for the phase function $p(\theta,\lambda)$ over the whole solid angle for wavelengths from 400 nm to 1000 nm the phase functions are normalized to a maximum of one. The logarithm of the intensity $\log(I(\lambda))$ is plotted against the negative cosine $-\cos(\theta)$ of the angle θ and the wavelength, see Fig. 13(a). We found that a rational equation fits the data

$$\log(p(x,\lambda)) = \frac{a+b\cdot x+c\cdot x^2+d\cdot\lambda}{1+e\cdot x+f\cdot\lambda+g\cdot\lambda^2}, \quad \text{with} \quad x=-\cos(\theta). \tag{13}$$

Parameters for the calculation of the phase function with Eq. 13 are given in Tab. 7 in the appendix for all measured fat emulsions. The absolute difference of the fit to the data shown in Fig. 13(a) can be seen in Fig. 13(b). The average relative error of the intensity of the fit is 4.5%.

4. Conclusion

The knowledge of the exact optical properties of fat emulsions is crucial for calibration tasks and the development of systems for diffuse optical tomography. Measurements of the optical properties, μ_a, μ_s, μ_s', g and $p(\theta)$, of six different fat emulsions were performed. The absorption

#92339 - $15.00 USD Received 1 Feb 2008; revised 18 Mar 2008; accepted 4 Apr 2008; published 11 Apr 2008
(C) 2008 OSA

coefficient of the fat emulsions was calculated from the water and soy bean absorption as was explained in section 3.5. The optical properties of the six fat emulsions were completely defined for VIS and NIR wavelengths.

The differences in μ_s, g and $p(\theta)$ of the different brands are significant and bigger than the standard deviations measured for different bottles of the same brand and concentration. Interestingly, also the same brands with different fat concentrations have significant differences in μ_s, g and $p(\theta)$ when diluted to the same fat concentration. Our measurements of μ_s, g and $p(\theta)$ of Intralipid 10 % shows large deviations to the measurements of van Staveren in 1991 [5]. This may be explained by changes in the recipe and the manufacturing of Intralipid since 1991. Interestingly the measurements of the reduced scattering coefficient of Intralipid 10 % are in good agreement with van Staverens findings. The significant deviations of μ_s and g do just compensate each other when calculating the reduced scattering coefficient with $\mu_s' = (1-g)\mu_s$. Also all other fat emulsions show a similar reduced scattering coefficient when diluted to the scatterer concentration of Intralipid 10 %.

We introduced method to calculate the particle size distribution by fitting Mie theory calculations to the phase function measurements and to collimated transmission measurements simultaneously. We computed the particle size distribution of six different emulsions. With the knowledge of the particle size distribution the optical properties, μ_s, μ_s', g and the phase function, were calculated with Mie theory. The calculations match the measurements reasonable well in the range of the measurement accuracy. With this method it was possible to calculate the optical properties also for wavelengths, at which no measurements have been performed. In comparison to standard methods for the particle size distribution measurement we got a more realistic result for the particle size distribution which could explain the optical properties well. Since the calculation with Mie theory is complicated, we introduced simple equations for the calculation of μ_a, μ_s, μ_s', g and $p(\theta)$ for unpolarized light. We presented parameters for six different fat emulsions for calculating the optical properties and the phase function with these equations for wavelengths from 400 nm - 900 nm in the appendix.

5. Appendix

Parameters for the calculation of μ_s, μ_s', μ_a, the phase function and the anisotropy coefficient are given in tables 3, 4, 5, 6 and 7 for unpolarized light respectively. The scattering and reduced scattering coefficient are calculated for the undiluted sample. For example, Intralipid 10% which consists of 100 g/l soy bean oil with a density of 0.927 g/ml and 12 g/l egg lipid is given for 12.0% scatterer concentration and Intralipid 20% is given for 22.8% scatterer concentration.

Tab. 3. Parameters for the calculation of the g-factor with Eq. 9 ($g(\lambda) = y_0 + a \cdot \lambda$, λ [nm], g) and the corresponding residual r^2 of the fit.

	Lipovenoes 10%	*Lipovenoes* 20%	*ClinOleic* 20%	*Intralipid* 10%	*Intralipid* 20%	*Intralipid* 30%
y_o	1.075E+0	1.085E+0	1.070E+0	1.018E+0	1.090E+0	1.066E+0
a	-6.079E-4	-6.029E-4	-6.369E-4	-8.820E-4	-6.812E-4	-4.408E-4
r^2	9.997E-1	9.992E-1	9.999E-1	9.926E-1	9.995E-1	9.982E-1

#92339 - $15.00 USD Received 1 Feb 2008; revised 18 Mar 2008; accepted 4 Apr 2008; published 11 Apr 2008
(C) 2008 OSA

Tab. 4. Parameters for the calculation of the scattering coefficient with Eq. 10 ($\mu_s(\lambda) = a \cdot \lambda^b$, λ[nm], μ_s[mm^{-1}]) and the corresponding residual r^2 of the fit.

	Lipovenoes 10%	*Lipovenoes* 20%	*ClinOleic* 20%	*Intralipid* 10%	*Intralipid* 20%	*Intralipid* 30%
a	1.576E+8	3.116E+8	3.468E+8	4.857E+8	3.873E+8	2.645E+8
b	-2.350E+0	-2.337E+0	-2.381E+0	-2.644E+0	-2.397E+0	-2.199E+0
r^2	9.994E-1	9.995E-1	9.995E-1	9.996E-1	9.995E-1	9.994E-1

Tab. 5. Parameters for the calculation of the reduced scattering coefficient with Eq. 11 ($\mu_s'(\lambda) = y_o + a \cdot \lambda + b \cdot \lambda^2$, λ[nm], μ_s'[mm^{-1}]) and the corresponding residual r^2 of the fit.

	Lipovenoes 10%	*Lipovenoes* 20%	*Intralipid* 10%	*Intralipid* 20%	*Intralipid* 30%
y_0	3.957E+1	7.723E+1	4.957E+1	8.261E+1	9.888E+1
a	-5.973E-2	-1.131E-1	-9.063E-2	-1.288E-1	-1.313E-1
b	2.743E-5	5.122E-5	4.616E-5	6.093E-5	5.702E-5
r^2	9.995E-1	9.996E-1	9.984E-1	9.996E-1	9.996E-1

Tab. 6. Parameters for the calculation of the absorption coefficient with Eq. 12 ($\mu_a = a / \left(1 + e^{-\frac{\lambda - x_0}{b}}\right)$, λ[nm], μ_a[mm^{-1}]) and the corresponding residual r^2 of the fit.

	a	b	x_0	r^2
water	3.066E+5	5.413E+1	1.770E+3	0.9508
soy bean oil	1.171E+5	-3.659E+1	-3.210E+2	0.9968

Tab. 7. Parameters for the calculation of the phase function $p(\lambda, \theta)$ with Eq. 13 ($\log(p(x,\lambda)) = \frac{a + b \cdot x + c \cdot x^2 + d \cdot \lambda}{1 + e \cdot x + f \cdot \lambda + g \cdot \lambda^2}$, $x = -\cos(\theta)$, λ[nm], θ[°], p[a.u.]) and the corresponding residual r^2 and standard error of the fit Std_{err}, which is defined by $Std_{err} = \sqrt{S_{err}/X_N}$, with X_N the degrees of freedom and S_{err} the sum of squares of the error.

Param.	*Lipovenoes* 10%	*Lipovenoes* 20%	*ClinOleic* 20%	*Intralipid* 10%	*Intralipid* 20%	*Intralipid* 30%
a	-2.741E+0	-2.109E+0	-2.898E+0	-6.395E-1	-1.913E+0	-3.098E+0
b	-1.765E+0	-1.433E+0	-1.809E+0	-2.807E-1	-1.292E+0	-1.898E+0
c	8.409E-1	5.837E-1	9.594E-1	3.940E-1	6.000E-1	8.463E-1
d	2.757E-4	2.175E-4	2.584E-4	-4.518E-5	1.079E-4	5.581E-4
e	2.632E-1	2.409E-1	2.338E-1	-1.574E-1	1.854E-1	3.049E-1
f	-5.570E-4	-1.268E-3	-2.899E-4	-2.369E-3	-1.423E-3	-5.019E-4
g	2.377E-6	2.458E-6	2.477E-6	2.927E-6	2.857E-6	1.540E-6
r^2	9.967E-1	9.933E-1	9.975E-1	9.657E-1	9.945E-1	9.936E-1
Std_{err}	4.465E-2	6.586E-2	3.694E-2	9.161E-2	5.503E-2	7.430E-2

Acknowledgment We like to thank Fresenius Kabi for the donation of Intralipid 10% and Intralipid 20%, Fabrizio Martelli for the valuable discussion and the donation of the Intralipid 30% sample. This work is supportet from the Landesgraduiertenförderung des Landes Baden-Württemberg and the Deutsche Forschungsgesellschaft (DFG).

#92339 - $15.00 USD Received 1 Feb 2008; revised 18 Mar 2008; accepted 4 Apr 2008; published 11 Apr 2008
(C) 2008 OSA